JOURNAL OF MATERIALS SCIENCE 14 (1979) 1269–1279

The structure of splat-quenched cadmium–zinc alloys

P. G. BOSWELL*, G. A. CHADWICK†
Department of Mining and Metallurgical Engineering, University of Queensland, St. Lucia, Queensland 4067, Australia

Splat-quenched Cd–Zn alloys having less than ≃35 at % Zn and less than ≃15 at % Cd solidify without solute partitioning at the highest cooling rates that can be attained using a room-temperature substrate. Lower cooling rates yield fine-grained microduplex structures possibly resulting from interdendritic precipitation or from the independent nucleation and growth of the terminal Cd and Zn phases. A further reduction in the cooling rate gives a transition from microduplex to lamellar eutectic solidifcation in the eutectic (Cd–26.5 at % Zn) alloy.

1. Introduction

The solidification of metal alloys by splat-quenching methods has frequently led to large metastable extensions of terminal solid solutions in binary systems that obey the Hume–Rothery conditions [1]. However, Duwez [2] reported that Cd–Zn alloys, which fulfil these conditions, did not form metastable solutions since X-ray diffractometry only showed the presence of equilibrium terminal phases in foils that had been quenched to, and held at, 97 K. Subsequently, Baker and Cahn [3] found, by the same technique, a small extension of up to 5 at % Cd in Zn and an unspecified but "appreciable" [4] extension of the Cd terminal solution. Several authors [5, 6] have argued that large extensions are lacking because the T_0 lines for the terminal Cd and Zn phases are very steep. T_0 is the temperature at which both solid and liquid of a given composition have the same free energy and it is the maximum temperature for composition-invariant (non-partitioning, "diffusion less" or "massive") solidification. Indeed Massalski *et al.* [6] have specified that appropriate T_0 lines for Cd–Zn alloys (see Fig. 1) gave a T_0 temperature of ≃300 K for Cd ≃ 20 at % Zn and Cd ≃ 90 at % Zn alloys. Accordingly, these two compositions represent approximate estimates of the maximum solid solubility limits that can be realized by splat-quenching Cd–Zn alloys onto a room temperature substrate.

Electron metallographic, unlike X-ray techniques can, in principle, resolve small amounts of metastable phases and are, therefore, more suited for determining extension limits in splat-quenched foils. Morever, the melting points of Cd–Zn alloys are low (<700 K) so it is likely that metastable phases will decompose during cooling from the solidification temperature. Consequently, it may be necessary to infer the terminal phase extension limits by examining the morphological

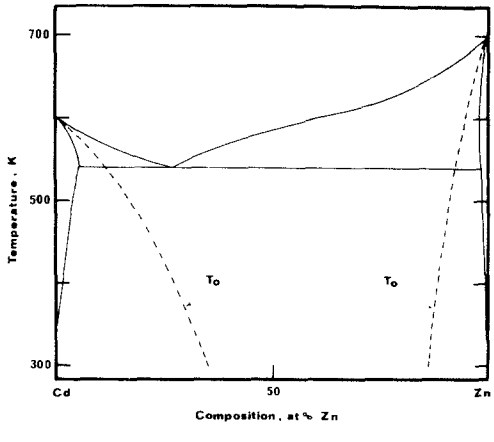

Figure 1 Cd–Zn phase diagram with schematic T_0 lines.

*Present address: Dental School, University of Queensland, Turbot St, Brisbane, 4067, Australia.
†Present address: Department of Mechanical Engineering, University of Southampton, Highfield, Southampton, UK.

characteristics of decomposed structures. This procedure would only be possible if adequate metallographic information were available.

This paper describes the results of an electron metallographic examination of splat-quenched Cd–Zn alloys which was undertaken in order to determine the microstructural characteristics of solidification products formed at high cooling rates. Particular care was taken to identify massively solidified (and subsequently decomposed) structures in concentrated alloys in order to critically examine the concept that steep T_0 lines restrict solid solubility limits in splat-quenched Cd–Zn alloys.

2. Experimental details

Alloys were prepared by melting and casting high purity (>99.999%) Cd and Zn in quartz tubes that had been evacuated to 10^{-5} Torr and back-filled with half an atmosphere of high purity argon. Pieces (≃200 mg weight) of the alloys were splat-quenched onto a polished copper substrate by the "gun" technique [7]. Back-filling of the evacuated quenching chamber with argon and short melting times (≃20 sec) to a maximum superheat of ≃150 K ensured a minimum amount of Cd and Zn vaporization. The alloy charges were melted in recrystallized alumina crucibles and they were expelled through a 1 mm diameter orifice by means of pressure waves created by the fracturing of 0.05 mm thick Mylar diaphragms with metered amounts of high purity helium.

X-ray powder specimens were prepared by glueing the thinner parts of the splat-quenched foils onto glass slides and they were examined using monochromated Cu$K\alpha$ radiation with pulse-height analysis. Two types of continuous X-ray scans were initiated within 5 min of splat-quenching, namely (i) repeated rapid scans at $1/2^\circ\,\text{min}^{-1}$ across selected low-order reflections, and (ii) single slow scans at $1/4^\circ\,\text{min}^{-1}$ across selected high-order reflections having 2θ diffraction angles greater than 90°. The former scans monitored any room-temperature transformation of the as-quenched alloys while the latter scans gave diffraction data for the determination of accurate lattice parameters. Randomly selected pieces of the splat-quenched foils were metallographically examined using optical and electron microscopy. The latter was in some cases initiated within an ageing time of 5 min at room temperature. Both conventional and scanning transmission (CTEM and STEM) techniques were used as well as secondary electron scanning microscopy (SEM).

3. Results

3.1. X-ray diffraction

The only phases that could be detected in the splat-quenched foils were Cd- and Zn-rich hexagonal close-packed solid solutions. For convenience, these solutions will be referred to as "extended" and "terminal" phases if they have compositions that are greater than or less than, respectively, the equilibrium solid solubility limits at the eutectic temperature, T_E. The experimentally determined lattice parameters are listed in Table I together with cell data for equilibrated alloys. The parameters obtained in this study were those calculated by at least-squares refinement of diffraction data measured following a standard room temperature ageing treatment of 30 min.

Examination of the tabulated parameters indicates that, within experimental error, the only extended solid solution that could be detected was the Cd-rich solution in a splat-quenched Cd-12.5 at % Zn alloy. The stability of this Cd-rich phase at room temperature was investigated by the rapid scan method. It was found that the Cd cell volume increased from 0.0430 ± 5.10^{-4} nm^3 after 10 min ageing at room temperature to 0.043156 ± 1.10^{-5} nm^3 after 30 min at the same temperature.

The alloy composition dependence of the texturing of the splat-quenched foils was investigated by comparing normalized intensity ratios for sets of reflections produced by a given phase. The ratios were calculated by dividing the intensity of the (0 0 . 2) reflection by the intensities of ($h\,k\,.\,l$) reflections. The intensities were, in all cases,

TABLE I Unit cell volumes for splat-quenched and equilibrium Cd–Zn alloys

	Cell volume (nm^3 × 10^6)	
	Cd solid solution	Zn solid solution
Splat-quenched		
Cd	43167 ± 10	—
12.5 at % Zn	43156 ± 10	30500 ± 40
33.3 at % Zn	43160 ± 20	30570 ± 50
50.0 at % Zn	43150 ± 30	30400 ± 20
75.0 at % Zn	43150 ± 25	30530 ± 30
87.5 at % Zn	43200 ± 25	30488 ± 10
Equilibrium [8]		
Pure metal	43180 ± 8	30419 ± 8
At solubility limit	43180 ± 8 (5.0 at % Zn)	30584 ± 15 (1.3 at % Cd)

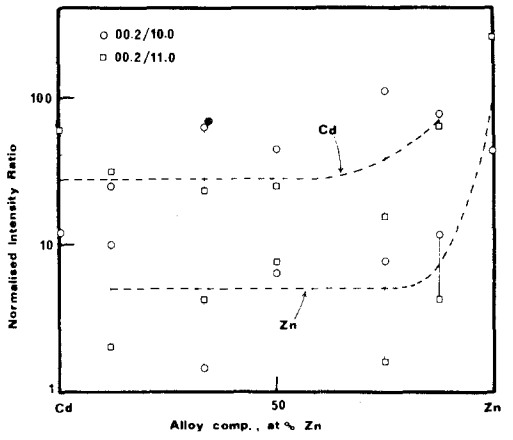

Figure 2 Observed texture parameters for splat-quenched Cd–Zn alloys.

determined after 30 min ageing at room temperature, and they were measured using a planimeter. The computed ratios were then normalized by dividing them by the equivalent ratios for well-annealed powders. Hence, the texturing parameter for say the $(h\,k\,.\,l)_{Cd}$ reflection is $\{(0\,0\,.\,2)/(h\,k\,.\,l)\}_{splat}/\{(0\,0\,.\,2)/(h\,k\,.\,l)\}_{powder}$. The presence of any $(0\,0.2)_{Cd}$ preferred orientation in a splat-quenched foil would give a value of the texture parameter that was greater than unity.

The observed texture parameters for (1 0.1) and (1 0.0) reflections are plotted in Fig. 2 on a logarithmic scale as a function of alloy composition. It can be seen that all the splat-quenched alloys displayed a strong (0 0.2) texture and that the degree of texturing increased as the alloy composition approached pure Zn. A similar tendency for a preferred orientation of close-packed crystal planes in the plane of the foil has been reported to occur in splat-quenched f c c alloys [5]. Texturing of this type probably arises as a result of either preferred surface nucleation of crystals having close-packed planes parallel to the foil surface and/or the preferred growth of those crystals having this same orientation. However, a consistent interpretation of the pronounced increase in texturing observed on increasing the Zn concentration cannot be given at the present time.

3.2. Metallography

Three types of microstructures were identified in the splat-quenched Cd-Zn foils. These were (a) eutectic structures; (b) microduplex structures comprising polycrystalline aggregates of the terminal Cd and Zn phases; and (c) two-phase structures comprising homogeneously distributed solute-rich precipitates in a polycrystalline solvent-rich matrix.

3.2.1. Eutectic structures

Fig. 3a shows an optical micrograph of an oblique section through a thick ($\simeq$30 μm) foil of a eutectic Cd–26.5 at % Zn alloy. Those foil regions well removed from the substrate are seen to contain eutectic grains with a regular lamellar structure. There are also a few small and roughly spherical particles of the primary Cd phase embedded within the eutectic grains. Each of these primary particles did not develop into a eutectic grain suggesting that solid Cd does not provide an efficient nucleating substrate for Zn. Measurements [9] of heterogeneous nucleation tempera-

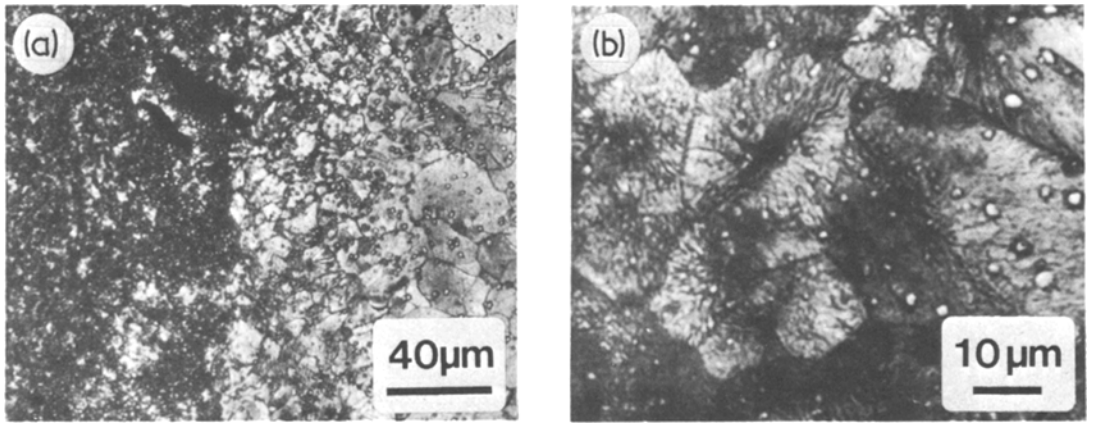

Figure 3 Lamellar eutectic structure in a splat-quenched eutectic Cd–26.5 at % Zn alloy. (a) Optical micrograph of an oblique section through a 30 μm thick specimen showing eutectic grains and microduplex material (left hand side of micrograph is located nearest the foil-substrate surface): (b) Enlargement showing several eutectic grains.

tures in entrained droplets support this conclusion. It was observed, using enlargements (Fig. 3b) of micrographs of typical eutectic grains, that the minimum interlamellar spacing in splat-quenched Cd–Zn eutectic alloys was $0.20 \pm 0.02\,\mu m$. The extrapolation of reported data [10] indicated that the spacing corresponded to growth at a maximum undercooling of 13 K below T_E with a maximum velocity of $7.10^{-4}\,m\,sec^{-1}$. Eutectic structures were only observed in the eutectic alloy and not in any of the other splat-quenched alloys examined.

3.2.2. Microduplex structures

Fig. 3a also demonstrates the observation that there was an abrupt transition from the lamellar eutectic structure to a very fine-grained structure. This fine-scaled structure was invariably found throughout the splat-quenched foils unless efforts were made to prepare relatively thick foils of the eutectic alloy. This is illustrated by Fig. 4a in which is given an optical micrograph of an oblique section through a splat-quenched eutectic alloy with the more normal foil thickness ($\simeq 10\,\mu m$). There are seen to be no eutectic cells and the fine-scale structure shows no discernible dendritic or columnar features. Fig. 4b shows a scanning electron micrograph of the surface of the foil imaged in Fig. 4a: the irregular outlines, the relative sizes and the arrangements of the constituent phases suggest that the microduplex structure comprised small Cd dendrites with interdendritic Zn particles (X-ray diffraction having indicated that no other phases were present in detectable amounts).

Microduplex structures were readily identified in electron transparent areas of all the binary alloys investigated. Using dark-field microscopy, electron beam microanalysis and selected-area electron diffraction techniques, it was established that the microduplex structures comprised aggregate mixtures of Cd and Zn grains. However, large variations were observed in the overall appearance (in bright-field) of the structures and the types of variations are illustrated in Fig. 5. This figure gives bright-field transmission electron micrographs which exemplify, collectively and individually, the following features of the microduplex material:

(a) considerable distortion in some areas of particular foils and almost no distortion in other areas. For example Fig. 5a and b were taken from different microduplex areas in a Cd–33.3 at % Zn foil: it can be seen that the grains shown in Fig. 5a display severe distortion while those shown in Fig. 5b represent a recovered, non-distorted structure.

(b) pronounced decreases in the average grain diameter as the alloy composition approached 50 at % Zn. This feature is illustrated in Fig. 5c showing a transmission electron micrograph of microduplex material observed in a Cd–50 at % Zn foil. The average grain size is only $0.01\,\mu m$ in contrast to the minimum average grain size of $0.5\,\mu m$ for splat-quenched pure Cd and pure Zn.

(c) an increased tendency for the formation of layered grains, at the expense of columnar grains extending through the foil, as the solute content increased. This feature is demonstrated in Fig. 5d and b. In the former figure the thin, layered grains in the Cd–50 at % Zn foil gave rise to numerous Moiré fringes at the grain boundaries. In the latter figure, the terminal-phase grains extend through the entire width of the Cd–33.3 at % Zn foil so

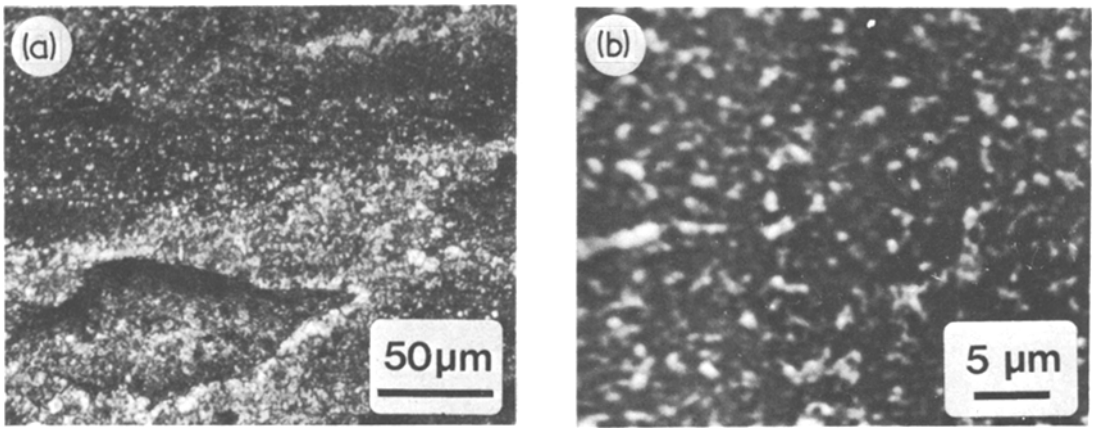

Figure 4 Microduplex structures; Cd–26.5 at % Zn alloy: (a) Oblique section through a $\simeq 10\,\mu m$ thick specimen: (b) SEM image of splat surface.

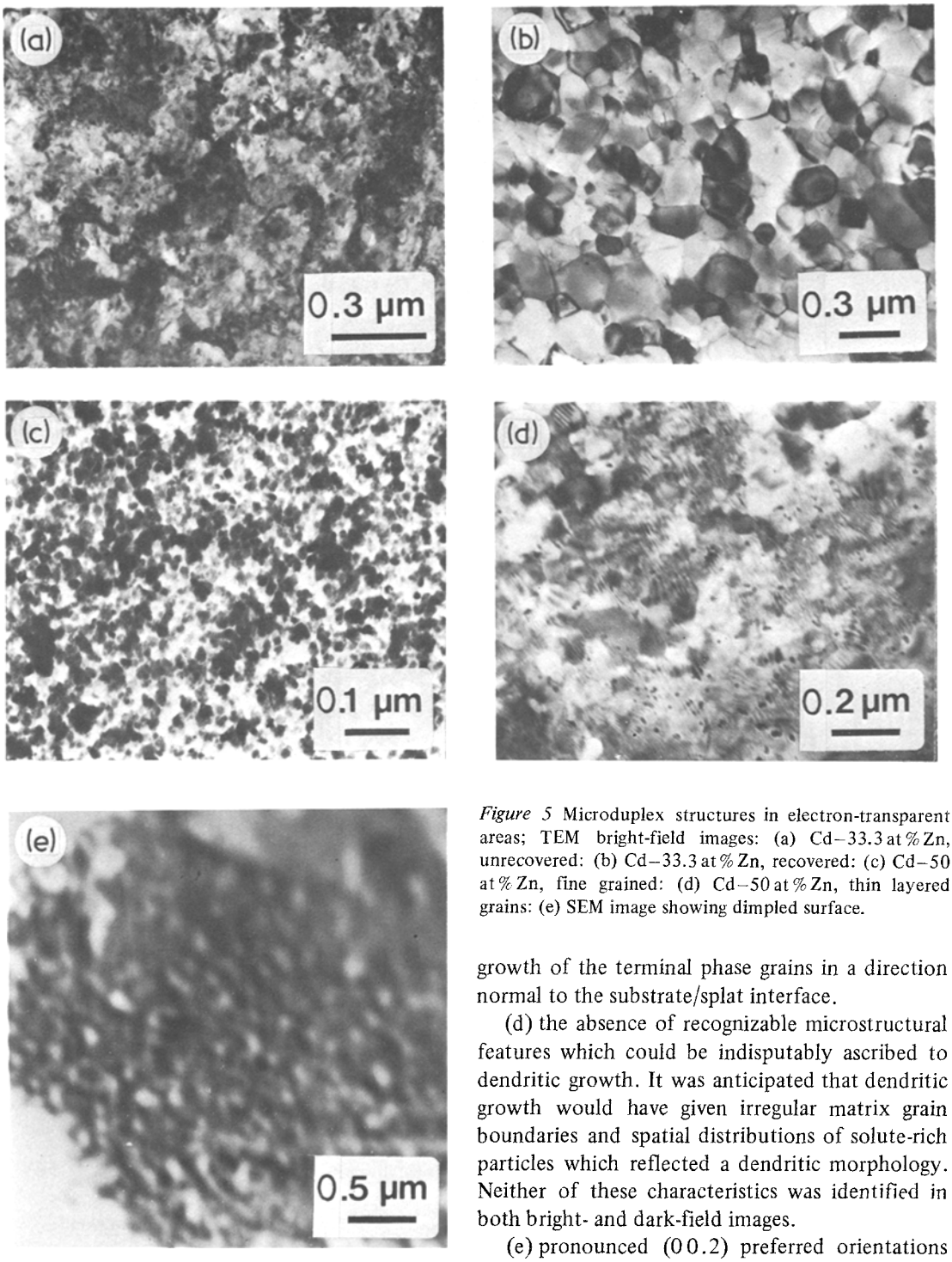

Figure 5 Microduplex structures in electron-transparent areas; TEM bright-field images: (a) Cd–33.3 at % Zn, unrecovered: (b) Cd–33.3 at % Zn, recovered: (c) Cd–50 at % Zn, fine grained: (d) Cd–50 at % Zn, thin layered grains: (e) SEM image showing dimpled surface.

very few grain-boundary fringes were imaged. The SEM image (Fig. 5e) of an area having a microduplex structure of the type shown in Fig. 5b indicated that the foil surface was dimpled. This effect probably arose as a result of the columnar growth of the terminal phase grains in a direction normal to the substrate/splat interface.

(d) the absence of recognizable microstructural features which could be indisputably ascribed to dendritic growth. It was anticipated that dendritic growth would have given irregular matrix grain boundaries and spatial distributions of solute-rich particles which reflected a dendritic morphology. Neither of these characteristics was identified in both bright- and dark-field images.

(e) pronounced (0 0.2) preferred orientations of the Cd and Zn phases with the (0 0.2) planes lying parallel to the foil surfaces.

3.2.3. Two-phase grains

Grains of a solvent-rich terminal solid solution having homogeneously distributed precipitates of a solute-rich terminal phase were detected in as-

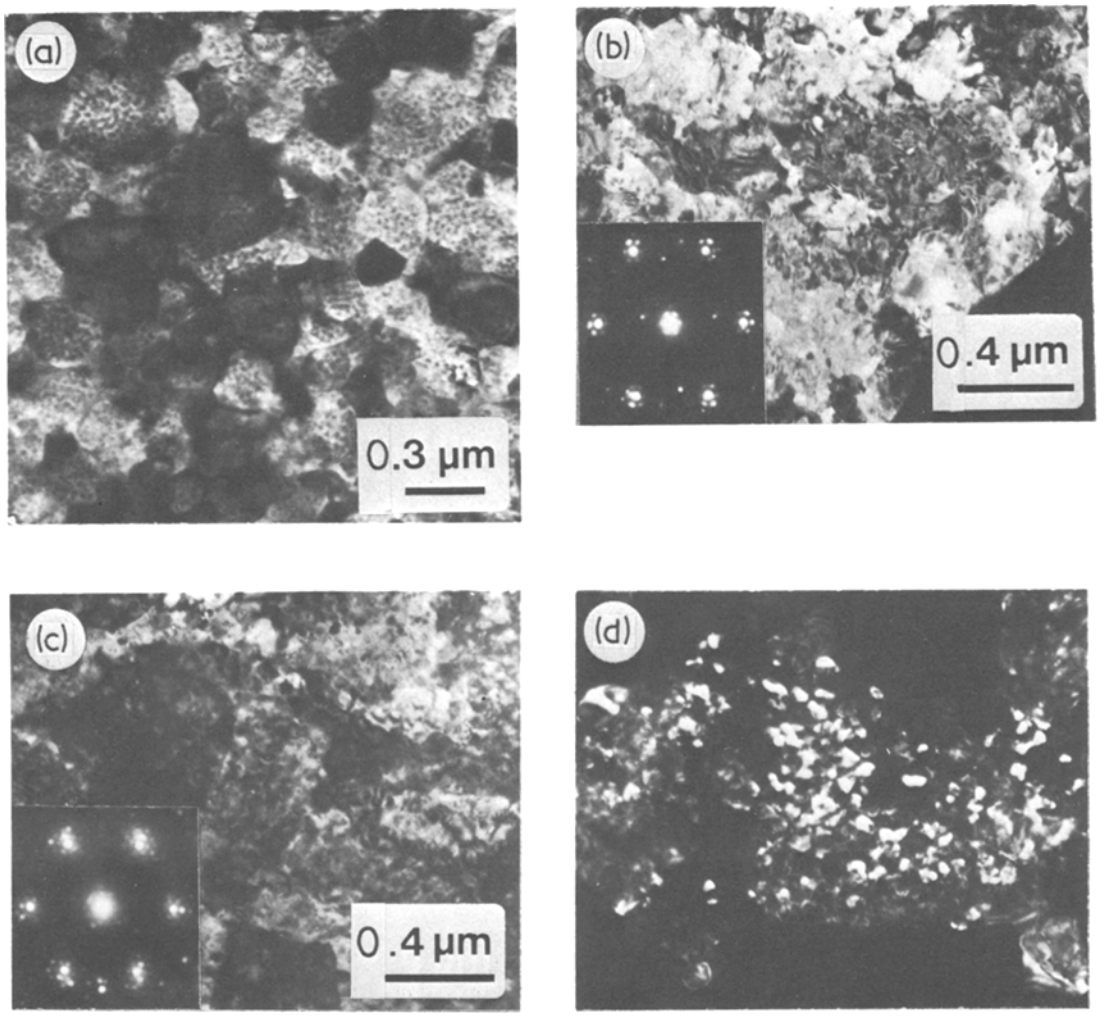

Figure 6 Two-phase (decomposed massive) structures: (a) Cd–12.5 at % Zn; (b) Cd–33.3 at % Zn; (c to e) Cd–26.5 at % Zn; (f, g) Cd–87.5 at % Zn: (a to c, f) TEM bright-field images; (d, g) TEM dark-field images; (e) STEM bright-field image (SBI/MBI conditions).

quenched foils of the Cd–12.5, 26.5, 33.3 and 87.5 at % Zn alloys but not in those of the Cd–50 and 75 at % Zn alloys. Bright-field electron micrographs of representative two-phase grain structures observed in foils of the Cd–12.5, 26.5, 33.3 at % Zn and 87.5 at % Zn alloys are shown in Fig. 6. The small, homogeneously distributed minor-phase particles were only clearly defined in Cd-rich alloys (e.g. Fig. 6a, Cd–12.5 at % Zn). Here it was found that the morphology of the two-phase structure was not destroyed during recovery, so undistorted grains having homogeneously distributed precipitates could be retained. In the remaining alloys which formed two-phase grains it was noted that the homogeneously distributed particles were only present in severely distorted material (e.g. Fig. 6b to g). Distortion generally masked contrast developed by the minor phase precipitates so these alloys required very detailed transmission electron metallography in order to detect the two-phase structures.

The selected-area diffraction patterns accompanying the bright-field images (Fig. 6) of the two-phase grains could each be indexed in terms of the terminal Cd and Zn phases with a well-defined basal–basal orientation relationship, namely $(00.2)_{Zn} \,||\, (00.2)_{Cd}$ with $\langle 11.0\rangle_{Zn} \,||\, \langle 11.0\rangle_{Cd}$. The numerous extra reflections evident in the patterns were attributed to double diffraction.

The matrix bend extinction contours, so evident in the bright-field images of the two-phase grains,

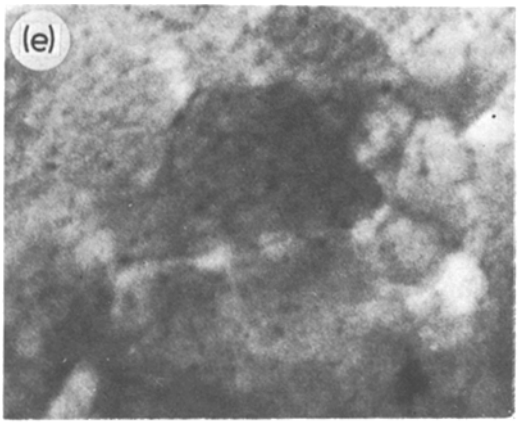

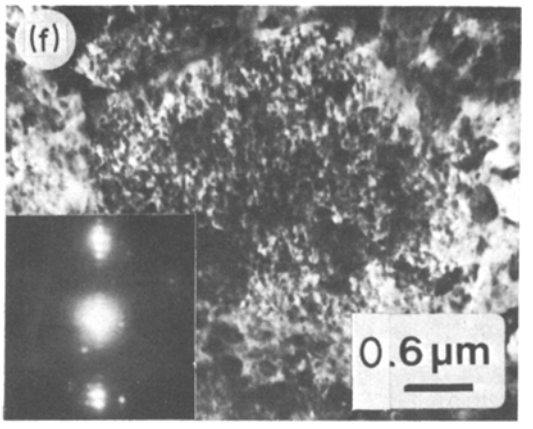

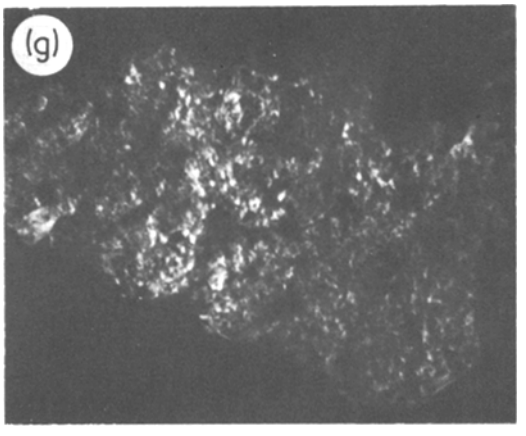

Figure 6 continued.

served to obscure the substructure of the grains. However, bend contours do not arise in dark-field images taken using precipitate reflections so the precipitate morphologies were examined in dark-field. Fig. 6 includes two examples of typical dark-field micrographs: in each case the precipitates imaged are those contained in the two-phase grains located at the centres of the accompanying bright-field images. The relative positions of the reflections that imaged the matrix grains and the precipitate particles indicated that the precipitates were solute-rich. The dark-field images themselves (e.g. Fig. 6d) showed that the precipitates in concentrated alloys often arose as thin plates having an irregular shape and $(0\,0.2)_{Zn} \,||\, (0\,0.2)_{Cd}$ habits. Scanning transmission electron microscopy (STEM) offers a suitable alternative imaging technique for removing extinction contour contrast and, unlike conventional dark-field imaging, preserves both matrix and precipitate contrast. The technique here is to record an STEM image using a large collector angle and an illumination angle that is greater than the smallest operating Bragg angle. These conditions have been termed [11] single-beam illumination (SBI) with multi-beam imaging (MBI). A STEM image (Fig. 6c) taken under these conditions accompanies the conventional bright- and dark-field images of Fig. 6c and d; the foil normal is parallel to the electron beam and the irregular regions of contrast within the matrix grains are the solute-rich (Zn) plate-like precipitates.

The overall microstructural characteristics of the two-phase grains observed in electron transparent areas deserve consideration. These grains usually arose in small clusters containing no more than about twenty grains. They were generally surrounded by microduplex structures showing considerable distortion. The matrix grain size of the two-phase grains was invariably larger than the average grain size of the surrounding microduplex material. Finally, the large two-phase grains always extended through the foil so that the grain boundaries were normal to the foil surfaces: layering of the grains was not observed. With regard to the precipitate morphologies, it was noted that there was no preferential formation of the minor-phase particles at grain boundaries. This observation, together with those relating to the crystallographic features of the two-phase grains, would indicate that the two-phase microstructure developed as a result of the uniform precipitation of solute-rich particles from a highly supersaturated matrix having little or no segregation. The initial, supersaturated matrix presumably arose as a result of composition-invariant, "massive" solidification in the Cd–12.5, 26.5, 33.3 and 87.5 at % Zn alloys.

Attempts to investigate the early stages of the decomposition of the massively solidified phases by TEM were unsuccessful. The precipitate structures described above were invariably well-developed after only 5 min ageing at room temperature (this being the minimum time required to mount a foil and locate a suitable two-phase microstructure). This rapid decomposition of the extended solid solutions confirmed the results obtained from the X-ray diffraction study of the rate of equilibration in splat-quenched Cd–12.5 at % Zn foils. However, it is worthwhile to note that there were no observations that could be used to distinguish between decomposition via a continuous (spinodal) or via a discontinuous (nucleation and growth type) process. The observations that (i) there were no precipitate-free zones adjacent to matrix grain boundaries; and (ii) the precipitates often appeared to have irregular, non-faceted outlines (as in Fig. 6d) could perhaps be cited as evidence for spinodal decomposition. However, because of the very large supersaturations involved it is also likely that precipitation via a nucleation and growth type process would produce these two observed features.

3.3. Energy dispersive X-ray microanalysis

The small grain size of the microduplex structure precluded a detailed study of solute profiles within individual grains. Hence the possibility that the terminal phase grains retained "cored" composition profiles as a result of dendritic growth was not investigated. The generally larger two-phase grains, however, could be microanalysed using the $\simeq$30 nm diameter STEM electron beam. It was found (a) that there were no significant composition variations within individual two-phase grains; and (b) that the average composition of two-phase grains was the same as that of surrounding microduplex material. Hence there was neither short-range segregation within two-phase grains nor long-range segregation between two-phase and microduplex areas. These results lend support to the proposal that the two-phase grains arose as a result of the decomposition of massively solidified solid solutions.

4. Discussion

The present study of splat-quenched Cd–Zn alloys has shown that there were straightforward progressions in the as-quenched microstructures with decreasing foil thickness, roughly equivalent to increasing cooling rate. Consider first the eutectic (26.5 at % Zn) alloy. It was established that relatively thick foils of this alloy contained lamellar eutectic grains (with embedded Cd primaries) and microduplex material. Thinner foils contained only microduplex material while a few isolated electron-transparent areas comprised microduplex structures surrounding aggregates of two-phase grains. It was concluded that the two-phase grains arose via decomposition, in the solid state, of a massively solidified h c p phase having the same composition as the alloy. This conclusion was based on the observed morphological features of the grains such as their larger size relative to the smaller average grain size of the surrounding microduplex material; their shape; the nature of their grain boundaries (straight or gently curved); their compositions as measured by microanalysis; and by their precipitate morphologies. This last consideration would include the uniform size and random distribution of the precipitates and their orientation relationship with the matrix.

The 12.5 at % Zn hypo-eutectic and the 33.3 and 87.5 at % Zn hyper-eutectic splat-quenched alloys contained microduplex and decomposed massive structures, but no lamellar eutectic nodules, while the 50 and 75 at % Zn alloys contained only microduplex material. These observations imply (i) that lamellar eutectic solidification in the splat-quenched alloys was restricted to a narrow range of undercoolings and alloy compositions located below and around the eutectic temperature and composition: and (ii) the maximum kinetic undercooling that could be achieved by splat-quenching was insufficient to produce massive solidification of the 50 and 65 at % Zn alloys at temperatures below their respective T_0 temperatures. Moreover, the volume fractions of the massively solidified products in the 33.3 at % Cd and 12.5 at % Zn alloys were very small. It is, therefore, likely that the use of a splat-quenching substrate maintained at 300 K limits massive solidification to alloys having less than $\simeq$35 at % Zn and less than $\simeq$15 at % Cd.

4.1. A solidification model for splat-quenched Cd–Zn alloys

The solidification behaviour of splat-quenched alloys can be analysed in terms of competing solidification reactions [12]. This approach involves the use of classical nucleation and growth theories

to calculate continuous-cooling-transformation (C-C-T) curves for the various reactions under the prevailing cooling conditions. These conditions should include the effects of recalescence which can be estimated by solving simultaneously the heat flow and solidification problems [13]. In constructing a C-C-T diagram for the eutectic Cd–Zn alloy it will be convenient to consider initially the solvent-rich Cd primary phase and the eutectic grains formed at low cooling rates, and the massively solidified structures formed at high cooling rates. The origins of the microduplex structures obtained at intermediate cooling rates can then be described in terms of the various models that have been proposed for microduplex solidification.

Metallography indicated that relatively thick foils of the splat-quenched Cd–Zn eutectic alloy contained small grains of the Cd-rich primary phase. The schematic C-C-T diagram of Fig. 7, therefore, shows a "start" of transformation curve for the nucleation and growth of a solvent-rich h c p phase. At low undercoolings the curve corresponds to the heterogenous nucleation of Cd primaries on impurity particles (and perhaps at foil surfaces) followed by dendritic growth with solute partitioning. At high undercoolings the curve corresponds to homogeneous nucleation followed by composition-invariant growth. This type of growth can be maintained if the solid–liquid interface temperature does not recalesce above T_0' during solidification. The temperature

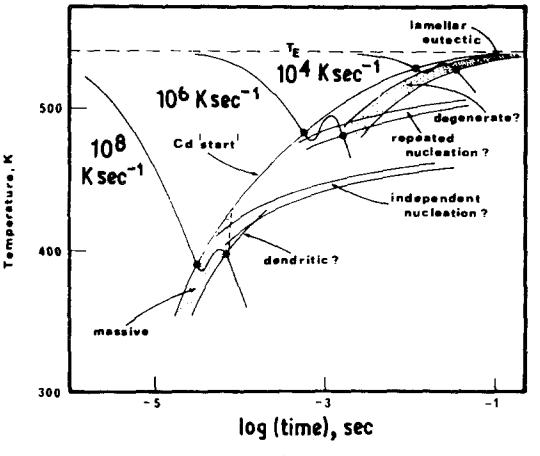

Figure 7 Continuous-cooling-transformation diagram for a splat-quenched eutectic Cd–Zn alloy: showing schematic "start" and "finish" curves and Newtonian cooling curves having the specified cooling rates at the eutectic temperature, T_E. Recalescence during solidification is illustrated schematically.

T_0' lies below T_0 and the difference between T_0 and T_0' corresponds to the driving force required by the interfacial kinetic processes. Therefore, we can draw a "finish" curve for complete solidification, below T_0', to a non-segregated massive structure. Cooling curves, which incorporate the effects of recalescence, can then be superimposed on the C-C-T diagram in order to demonstrate that completely massive structures develop above a critical cooling rate. Solidification at lower cooling rates is accompanied by solute segregation and the eventual formation of the Zn-rich solid solution.

It was established metallographically that at very low cooling rates, the Cd primaries formed in conjunction with lamellar eutectic grains. It is, therefore, reasonable to draw start and finish curves for eutectic solidification. Measurements of interlamellar spacings indicated that the maximum undercooling for lamellar eutectic growth was $\simeq 13$ K: the C-C-T curves for eutectic solidification are labelled accordingly. Quenching at rates below some critical rate, corresponding to the 13 K undercooling, yields lamellar eutectic grains whereas cooling at rates lying between the critical rates for lamellar eutectic and massive solidification produces microduplex structures.

4.2. Microduplex solidification

Several models have been proposed for microduplex solidification and they include the degenerate eutectic [14], the dendritic [15], the repeated nucleation [16] and the independent nucleation [17] models. The degenerate eutectic model postulates a transition from a regular to an irregular arrangement of the constituent phases of the eutectic grains. These phases are largely continuous in three dimensions but sections through degenerate structures may reveal a particulate morphology which could be mistaken for a microduplex structure. The regular-degenerate transition obtained on increasing the cooling rate may also be accompanied by a transition from planar to dendritic coupled growth [18]; and to a considerable refinement in the eutectic grain size. These two processes could make the identification of degenerate eutectic structures exceedingly difficult using optical and scanning electron microscopy. In the case of splat-quenched Cd–Zn eutectic alloys there appeared to be a relatively sharp transition from a coarse-grained, regular eutectic structure to a fine-grained microduplex

structure. This transition did not seem to involve the formation of a degenerate eutectic structure. However, any definitive discussion of the transition clearly requires additional metallographic information obtained using transmission electron microscopy.

The three remaining models for microduplex solidification attempt to relate the morphological features of the solvent-rich primary grains with the features developed during the solidification processes involving the precipitation of Zn. For example, the dendritic model invokes dendritic growth of the solvent-rich phase followed by interdendritic precipitation. Formal descriptions of the model can be developed in terms of coupled growth theory [19] and in terms of the degree of solute segregation during dendritic growth [15]. In the former approach, it is argued that dendritic solidification is favoured because dendritic growth is faster than co-operative eutectic growth. This is the case if the temperature and composition of the liquid alloy place it outside the so-called "coupled zone". It is reasonable to assume that the coupled zone for Cd–Zn is disposed symmetrically about the eutectic composition; and that any contraction of the zone due to kinetic factors [20] is negligible at the levels of kinetic undercoolings which can be developed in splat-quenching. In view of these considerations, it is perhaps surprising that eutectic growth appears to be suppressed with relative ease in Cd–Zn alloys. However, it must be noted that the coupled zone approach is not specific about nucleation. Indeed, the absence of eutectic structures in rapidly quenched alloys may simply be due to difficulties associated with the development of eutectic embryos. Unfortunately, any qualitative evaluation of the competition between eutectic and dendritic (microduplex) solidification would be invalidated by the uncertainties associated with the assumed models for the nucleation of eutectic grains.

The alternative approach used in developing the dendritic model is based on the concept that any suppression of solute segregation, during primary solidification, tends to reduce the opportunity for eutectic solidification. This would be the case if a substantial degree of massive solidfication occurred prior to recalescence, and subsequent dendritic growth, above T_0'. Indeed, microstructural observations made using Al-based eutectic alloys have shown that dendrites can develop from massively solidified cores [21]. The dendrites evidently grow to impingement prior to the formation of eutectic embryos. The formation of these partially massive, dendritic structures can be represented on the C-C-T diagram by drawing extensions to the massive solidification curves (see Fig. 7).

Efforts to demonstrate conclusively, the presence of dendritic structures in the splat-quenched Cd–Zn alloys were unsuccessful. However, the examination of foil surfaces by scanning electron microscopy revealed contrast variations reminiscent of dendritically segregated structures. Also, some electron-transparent areas were observed to contain aggregate mixtures of thin, layered Cd and Zn grains. The interphase and grain boundaries were largely parallel to based planes and to the foil surfaces. These layered structures may have arisen via the growth of branched dendrites normal to the foil surfaces followed by interdendritic precipitation of plate-like precipitates. The particulate morphology may then have developed during solid-state cooling.

Since these two sets of observations indicate that dendritic solidification occurred, it is perhaps surprising that partially massive structures were not observed in the splat-quenched Cd–Zn alloys. Instead, there appeared to be a transition from completely massive structures to structures comprising aggregate mixtures of columnar grains of the Cd and Zn phases. It is, therefore, necessary to consider briefly the two remaining models for microduplex solidification. The repeated nucleation model invokes growth of a microduplex colony by repeated surface nucleation. The model could perhaps be developed to provide plausible descriptions for the origins of several of the different types of microduplex structures. It may also be possible to estimate transformation curves similar to those shown schematically in Fig. 7, which quantify the competition between solidification via co-operative eutectic growth and via repeated nucleation.

Likewise, it is not unreasonable to consider competition between massive solidification of a solvent-rich phase and the independent nucleation and growth of both terminal phases. Effective competition would require that the start curve for Zn precipitation approaches the Cd primary start curve in the manner shown in Fig. 7. It is envisaged that nucleation of both phases may be catalysed at the splat-quenched foil surfaces so that it would not be necessary to undercool the eutectic alloy below the homogeneous nucleation temperatures

for both Zn and Cd. Subsequent growth may then take place normal to the foil surfaces to give the columnar microduplex structures observed in areas surrounding the decomposed massive structures.

5. Conclusions

An optical and electron metallographic study of splat-quenched Cd–Zn alloys prepared by the gun technique indicated that:

(a) Cd-rich alloys with less than about 35 at % Zn and Zn-rich alloys with less than about 15 at % Cd can be solidified massively (i.e. without solute partitioning) using a room temperature copper substrate;

(b) the massively solidified, extended, solid solutions decomposed rapidly at room temperature to give two-phase grains comprising homogeneously distributed, solute-rich, plate-like precipitates in a solvent-rich matrix;

(c) progressively larger quench rates gave lamellar eutectic, microduplex and decomposed massive structures in the eutectic (26.5 at % Zn) alloy;

(d) lamellar eutectic solidification was restricted to a narrow composition range ($\simeq$ 20 to 30 at % Zn) and to small ($<$ 13 K) undercooolings below the eutectic temperatures. Alloys solidifying outside this regime, but above their respective T_0' temperatures, formed microduplex structures.

(e) Microduplex structures in thick ($\simeq 10\,\mu m$) specimens appeared to develop via interdendritic precipitation while those observed in electron transparent areas may have resulted from the independent nucleation of both Cd and Zn solid solutions followed by columnar growth.

Acknowledgement

The authors are indebted to the Australian Research Grants Committee for supporting this research.

References

1. P. DUWEZ, R. H. WILLENS and W. KLEMENT, *J. Appl. Phys.* **31** (1960) 1136.
2. P. DUWEZ, *Prog. Solid State Chem.* **3** (1967) 377.
3. J. C. BAKER and J. W. CAHN, *Acta Met.* **17** (1969) 575.
4. B. C. GIESSEN, "The Crystal Chemistry of Metals and Alloys" (Interscience, New York, 1972) p. 287.
5. H. JONES, *Rep. Prog. Phys.* **36** (1973) 1425.
6. T. B. MASSALSKI, L. F. VASSAMILLET and Y. BIENVENU, *Acta Met.* **21** (1973) 649.
7. P. DUWEZ and R. H. WILLENS, *Trans. Met. Soc. AIME* **227** (1963) 362.
8. W. B. PEARSON, "Handbook of Lattice Spacings and Structures of Metals and Alloys" (Pergamon Press, London, 1958).
9. R. T. SOUTHIN and G. A. CHADWICK, *Acta Met.* **26** (1978) 223.
10. A. MOORE and R. ELLIOT, "The Solidification of Metals" (Iron and Steel Institute, London, 1967) p. 167.
11. T. YAMAMOTO and H. NISHIZAWA, *Phys. Stat. Sol.* **28A** (1975) 237.
12. P. G. BOSWELL and G. A. CHADWICK, *J. Mater. Sci.* **12** (1977) 1879.
13. *Idem, Scripta Met.* **11** (1977) 459.
14. M. J. BURDEN and H. JONES, *J. Inst. Metals* **98** (1970) 249.
15. T. Z. KATTAMIS and M. C. FLEMINGS, *Met. Trans.* **1** (1970) 1449.
16. W. A. TILLER, "Liquid Metals and Solidification" (American Society for Metals, Cleveland, 1957) p. 276.
17. L. M. SERGEEV, *Tsvet. Metally.* **14** (1974) 67.
18. M. F. CHELL and W. H. KERR, *Met. Trans.* **3** (1972) 2002.
19. C. ZENER, *Trans. AIME* **167** (1946) 550.
20. H. FREDRIKSSON, *Met. Trans.* **6A** (1975) 1658.
21. P. RAMACHANDRARAO, M. G. SCOTT and G. A. CHADWICK, *Phil. Mag.* **25** (1972) 961.

Received 20 June and accepted 13 October 1978.